Egyptian Journal of Chemistry

http://ejchem.journals.ekb.eg/

Novel In Situ Gel for Molnupiravir-Loaded Niosomes: Design, In Vitro Characterization and In Vivo Evaluation

Hadeer A. El- Hashemy[a]*, Abeer Salama[b], Amira Rashad[c]

[a]Pharmaceutical Technology Department, National Research Centre, El-Buhouth St, Cairo 12622, Egypt.
[b]Pharmacology Department, National Research Centre, El Buhouth St., Cairo 12622, Egypt.
[c]Pharmaceutics and Pharmaceutical Technology Dept., Faculty of Pharmacy, Heliopolis University, Cairo-Belbeis Road, Cairo, 11785, Egypt.

Abstract

Acute lung injury is a clinical disease that causes damage to the pulmonary capillary endothelium leading to a notable rate of morbidity. Clinical manifestations of SARS-CoV-2 infections vary; some persons remain asymptomatic, while others develop COVID-19, with mild to critical severity. Molnupiravir is an antiviral candidate with demonstrating efficacy against SARS-CoV-2. The present investigation aims at developing Molnupiravir thermosensitive in situ nasal gel for the treatment of acute lung and respiratory injuries with improved therapeutic efficacy. Niosome encapsulation efficiency, vesicle size, shape, and size distribution were investigated. The optimized niosomes, comprised of Span® 60 and cholesterol, displayed particle size of 92.215 ± 6 nm, zeta potential of -29.67 ± 0.22 mV and encapsulation efficiency of 95.36 ± 1.5%. The optimal nano-dispersion was incorporated into hydroxyethyl cellulose. The resulting gels showed pseudoplastic mucoadhesive appearance with a prolonged in vitro drug release pattern. Instillation of the Molnupiravir-loaded niosomal gel into rats' nasal cavity ameliorated lung damage via a reduction of the cytokine storms induced by potassium dichromate (TNF-α / TGF-β) . Molnupiravir-loaded niosomal gel elevated PI3K/ Akt signaling pathway which promoted cellular growth. Consequently, the invented nano-particulate gelling system may offer an appropriate carrier for better enhancement of serious respiratory disorders.

Keywords*:* Molnupiravir; Acute lung injuries; In situ nasal gel; Niosomes,; PI3K/ Akt; potassium dichromate.

1. Introduction

Serious morbidity rates are associated with acute lung injury (ALI), a common clinical disease that affects individuals as well as animals. ALI causes damage to the alveolar epithelial cells and pulmonary capillary endothelial cells, leading to the accumulation of plasma proteins and fluid in the air sacs. This leads to severe respiratory failure with low oxygen levels, infiltration of inflammatory cells, and the release of pro-inflammatory cytokines. In advanced cases, it progresses to acute respiratory distress syndrome (ARDS) [1]. ALI can result in life-threatening respiratory failure requiring mechanical ventilation, which increases the risk of multiple organ dysfunction and mortality [2]. Currently, supportive management with mechanical ventilation is the main approach, but the mortality rate remains high at around 30-40% [3]. Scientists have a pressing need to find superior medications for ALI and lessen its elevated fatality rate. Furthermore, it is worth noting that the severe acute respiratory disease, known as COVID-19, is caused by the novel severe acute respiratory syndrome Coronavirus 2 (SARS-CoV-2). SARS-CoV-2 has spread quickly around the world, sparking a pandemic as per World Health Organization (WHO), reporting nearly 260 million infections and 5.2 million deaths cases [4]. The antiviral ribonucleoside analogue b-D-N4-hydroxycytidine is the source of the prodrug molnupiravir. It has demonstrated efficacy in treating infections brought on by a variety of RNA viruses, such as encephalitic alphaviruses, influenza viruses, and highly deadly coronaviruses [5]. Upon administration, Molnupiravir quickly breaks down in the bloodstream to generate its active form, 5'-triphosphate, by host kinases [6]. Where it serves as an alternative substrate for viral RNA-dependent. RNA polymerase (RdRp) offering a competitive approach. When this substance binds with viral RNA, series of mutations are build up in the viral genome, eventually causes deadly mutations to appear [7]. This

*Corresponding author e-mail: hadeer_egy@hotmail.com.; (ha.el-hashemy@nrc.sci.eg).
Receive Date: 03 February 2024, Revise Date: 04 March 2024, Accept Date: 21 March 2024
DOI: 10.21608/ejchem.2024.267230.9279

mechanism functions through the concept of "error catastrophe," based on the idea that raising the mutation rate in the viral genome beyond a biologically sustainable threshold renders the virus unable to survive, resulting in its eradication [8]. Human airway epithelial cell cultures have showed the efficacy of molnupiravir against SARS-CoV-2[5]. The administration of Molnupiravir, both prophylactically and therapeutically, resulted in boosted lung health, reduced virus concentrations, and lowered body weight reduction in a study conducted on infected mice [9, 10]. Many preclinical and scientific researches showing a 50% decrease in COVID-19 hospitalizations and deaths support the safety and effectiveness of molnupiravir in treating SARS-CoV-2 infection [11-13]. Upon oral administration, esterases swiftly breakdown molnupiravir, giving it a half-life of about 3.3 hours [14]. Along with the aforementioned problem, diarrhea, nausea, vomiting, dizziness, and skin rash are among the several side effects of oral Molnupiravir that have been recorded [15]. The use of the nasal approach for is growing in popularity due to its effectiveness in achieving localized effects and its ability to compete with the gastrointestinal tract for systemic drug delivery [16]. This method offers a convenient and non-invasive approach to drug application and allows for self-administration; removing the negative consequences that intravenous is frequently linked with. Additionally, the nasal route has several benefits for systemic drug administration, such as a wide surface area for absorption, avoiding drug breakdown in the GIT, avoiding liver first-pass metabolism, and obtaining comparatively better bioavailability [17]. Niosomes as a vesicular nanosystem are composed of nonionic surfactants and have the ability to self-assemble [13]. The amphiphilic properties of surfactants in niosomes, which exhibit a lamellar bilayer structure, were encountered for boosting the solubility of hydrophobic drugs, exerting superior permeability across biological membranes, and having the potential to prolong drug accumulation in circulation [11, 12]. Therefore, the purpose of this work is to synthesize molnupiravir into a niosomal nasal in situ gel in order to increase its bioavailability while mitigating adverse effects of oral administration.

2. Materials and Methodology

2.1. Materials

Monlnupiravir donated as a gift by EPICO pharmaceutical company, Cairo, Egypt., Span 60® (Sp60), Span 40® (Sp40), hydroxyethyl cellulose (HEC) & cellulose membrane12 000–14 000 molecular weight cutoff : (MWCO) were bought through Sigma-Aldrich, St. Louis, USA, Cholesterol (97%) (CH) was delivered by Panreac, Barcelona, Spain, Propylene glycol and Chloroform; HPLC grade was obtained from Alpha Chemical, Mumbai, India. Methanol (HPLC grade, Fisher UK). Potassium dichromate was purchased from Sigma Aldrich,

TNF-α, TGF-β, PI3K and AKT ELISA kits were obtained from specific ELISA kit, Sunlong Biotech Co., Ltd, China. The rest of the compounds were all analytical quality.

2.2. Animals

Forty male Wister albino rats weighing between 140-150 g were obtained from the Animal House of the National Research Centre in Cairo, Egypt. The rats were housed in groups and kept in monitored conditions with a 12-hour light/dark cycle and a room temperature of 25 ± 2 °C. They were provided with standard laboratory rodent chow and water ad libitum. All animal experiments were conducted in compliance with the guidelines set by the Institutional Animal Ethics Committee (Medical Research Ethics Committee, MREC) of the NRC, Cairo, Egypt.

2.3. Methods

2.3.1. Experimental Design

Utilizing a 2^2 factorial experimental design, the impact of the distinct variables on the correlated responses was maximized.. The factors under investigation included X_1: Type of surface active agent (SAA) categorized as either Sp60 or Sp40 and X_2: Ratio of SAA to CH (Cholesterol) - with options of 1:1 or 1:2. The measured dependent variables encompassed Y_1: Entrapment Efficiency (EE, %), Y_2: Size of vesicles (VS, measured in nanometers), and Y_3: Zeta Potential (ZP, measured in millivolts). The details of the factor levels and corresponding responses can be found in Table 1. The analysis of the factors' effects on the dependent variables was conducted by Design-Expert® 8.0 software (Stat-Ease Inc., Minneapolis). A single-way ANOVA was used to evaluate the acquired data in order to determine the significance of the factors and their interactions with respect to the selected responses. A significance level below 0.05 was deemed statistically meaningful.

Table 1: Individual variable levels & responses

Independent variables (factors)	***Levels***	
X_1: SAA type	Sp40	Sp60
X_2: SAA:CH ratio	1:1	1:2
Dependent variables (responses)	***Constraints***	
Y_1: Entrapment efficiency (EE %)	Maximize	
Y_2: Vesicle size (nm)	Minimize	
Y_3: Zeta Potential (mV)	Maximize	

2.3.2. Synthesis of Niosomes Loaded with Molnupiravir (Mol-Ns)

Mol-Ns (Mol-containing niosomes) were formulated through thin film-hydration technique, employing diverse blends of nonionic surfactants and cholesterol at varying ratios. Detailed compositions of the resulting niosomes can be referenced in Table 1. In order to develop the niosomes, a specific amount of the drugs (20 mg), the chosen SAA, and cholesterol were dispersed in a 3:1 v/v solution of methanol and chloroform in a flask with a circular bottom. Following the evaporation of organic solvents using a rotary evaporator at 60°C for an hour, a film coated the inner surface of the flask was formed. Subsequently, to moisten the dried film, ten milliliters of distilled water were added. This process occurred over 60 minutes at 60°C, rotating at 50 rpm. The resulting suspension was then left to mature fully overnight in a refrigerator to achieve complete development.

2.3.3. Characterization of Mol-Ns

2.3.3.1. Entrapment efficiency (EE%):

The entrapment efficiency percentage of Molnupiravir enclosed within the niosomes was assessed indirectly. This was achieved by gauging the spectrophotometric absorbance of the un-encapsulated drug using spectrophotometer (Shimadzu-50–02, Kyoto, Japan) set at a wavelength of 250 nm. To evaluate the EE%, distilled water was used to dilute a 1 ml sample of the freshly manufactured Mol-Ns dispersion to 10 ml. This mixture underwent high-speed cooling centrifugation at 9000 rpm and 4°C for one hour using a Union 32R centrifuge (Hanil Science Industrial Co., LTD, Korea). Pellets and the remainder of the free drug solution are separated by centrifugal. After another round of centrifugation, the particles were re-suspended in distilled water to wash out any remaining drug. Following collection, spectrophotometric analysis was performed on the supernatant. The following calculation was adopted to assess EE %

$$\text{EE \%} = \frac{\text{Total amount of Mol−free Mol}}{\text{Total amount of Mol}} \times 100 \quad (1)$$

2.3.3.2. Vesicle Size (VS)

Laser diffraction technique was manipulated using Malvern Zetasizer (Malvern Instruments, Worcestershire, UK) to assess niosomes mean vesicles size. The sample volume of half a milliliter was blended with 10 ml of distilled water in order to achieve the desired scattering intensity. Each sample's VS were tested in triplicate at 25 °C.

2.3.3.3. Zeta potential measurements (ZP)

The vesicles charges values were recorded by Malvern Zetasizer using same procedure as mentioned under section 2.3.2.2.

2.3.3.4. Gel preparation (Mol-NGs)

A batch of Mol-NG (10 g) was formulated by blending niosomal dispersions, ≈ to 2% of Mol (w/w), with the aqueous phase of HEC (gel-forming excipient). This amalgamation underwent magnetic stirring for 30 minutes until reaching a uniform consistency. Subsequently, the mixture was stored at 3–5 °C for future utilization.

2.3.3.5. In vitro release study

Employing a water bath with a thermostat and a dialysis bag, molnupiravir release patterns were examined (Memmert, SV 1422, Schwabach, Germany). Samples for the drug release research included free drug solution, 1.0 g of the chosen Mol-NG and the appropriate Mol-N dispersion (10 mg Mol), which were put into dialysis bags that were sealed on both ends. Bags were kept at 37±0.5 °C by being submerged in 50 milliliters of phosphate buffer pH 6.8, which was agitated at 100 rpm. Two milliliter samples were taken at predetermined intervals and promptly refilled with an exact quantity of fresh phosphate buffer pH 6.8 so as keep the sink conditions [18]. The drug content of the removed samples was then measured via spectrometer at 250

nm. Plotting the cumulative % of medication released versus time was done. Every measurement was done three times, and the mean ± SD was computed.

2.3.3.6. Transmission electron microscope (TEM)

The morphological characteristics of the niosomal dispersions were examined via TEM (JEM-2100, Tokyo, Japan). On a copper grid coated with carbon, a drop of the tested formula was applied and stained with a 1% sodium phosphotungstate solution. Using absorbent filter paper, extra fluid was collected, and the sample was dried at 25°C for three minutes [19].

2.3.3.7. Rheology study

A digital rheometer (Physica MCR 301, GmbH) with a cone and plate conformation (plate dimensions 40 mm, 4° cone angle) was used to test the rheological attributes at a temperature of 25°C ± 0.1. Viscosity and flow curves for the chosen Mol-NGs were recorded over a total of six minutes. The shear rate was progressively increased during the ascending period from 1 to 400 s^{-1} over duration of 3 minutes. Then, during the next three minutes of the descending phase, the shear rate declined from 400 to 1 s^{-1} [20]. All measures were tripled.

2.3.3.8. Determination of pH

One gram of the prepared gels was diluted with distilled water in a 10 ml volumetric flask, and the resulting solution was further diluted with distilled water. A pH tester was utilized to find the solution's pH degree (Bibby Scientific Limited, UK) previously calibrated using phosphate buffers at pH 4 and pH 7 [20].

2.4. In vivo testing

2.4.1. Experimental design

Four groups of forty rats (n = 10) were randomly assigned. Group I was the control group and was administered saline intranasally (i.n.). Group II was administered a single dosage of 2 mg/kg of potassium dichromate ($K_2Cr_2O_7$) through the nose, serving as a model group for ALI. Group III: given intranasal $K_2Cr_2O_7$, followed by a 24-hour administration of Molnupiravir (4 mg/ml)[21] . Group IV: 200 µl of the selected niosomal gel (containing 2 mg of drug concentration per nostril, for a total of 400 µl to 4 mg of Molnupiravir) was given to them after they had intranasal $K_2Cr_2O_7$ for 24 hours.

2.4.2. ***Measurement of AKT, PI3K, TGF-β, and TNF-α***

Under minimal anesthesia, the animals were sacrificed by being decapitated. Following a saline wash, the lung was homogenized (20%) using a tissue homogenizer (BitLab Medical, MPW-120, Poland) in icy phosphate buffer (pH 7.4). The tissues were then centrifuged using a cooling centrifuge (2 K15, Sigma Co., Germany) at 4000 rpm/min for 10 min at 4°C. ELISA strips (Sunlong Biotech Co., Ltd., China) were utilized to measure the lung contents of TNF-α, TGF-β, PI3K, and AKT after the supernatant was collected and kept at -80 °C [22].

2.4.3. Histopathology analysis

The lungs of the rats in multiple groups were autopsied, as the tissues remained for a full day in 10% formol saline. With methyl, ethyl, and 100% ethyl alcohol dilutions, the animals were dehydrated following a tap water wash. The samples underwent a twenty-four-hour paraffin immersion at 56°C in a hot air oven following their cleaning in xylene. Using a rotating LEITZ microtome, tissue blocks made of paraffin beeswax have been generated for sectioning at a thickness of 4µ. To facilitate further analysis, the tissue sections that resulted were put on glass slides, deparaffinized, and stained with hematoxylin and eosin [23].

2.5. Statistical Analysis

Three duplicates of each experiment were carried out, and the outcomes were depicted as mean values with their corresponding standard deviations (mean ± SD). Using GraphPad Prism 5 Software version 5 (San Diego, CA), one-way analysis of variance (ANOVA) and the Tukey multiple comparisons test were used to assess statistical differences. A significance threshold of $p < 0.05$ was employed for determining statistical significance.

3. Results and discussion

3.1. Synthesis and factorial design of Mol-NGs

Thin-film hydration was adopted to create molnupiravir-loaded niosomes by mixing various sorts of SAA (Sp40, Sp60) at various ratios with CH. A range of molar ratios of SAA/CH, from 1:1 to 1:2, were used to synthesize niosomes. The entirety of the prepared Mol-Ns formulations exhibited uniform and homogeneous dispersions, devoid of any detectable aggregations. Four Mol-Ns were inspected as per the experimental protocol; Table 2 lists their compositions and results. Furthermore, Design Expert software® was exploited to generate figures that illustrate the impact of independent factors and their possible interactions on the VS, ZP, and EE% (see figure 1).

3.2. Characterization of Mol-Ns

3.2.1. Composition Variables' Impact on the EE% of Mol-Ns

As clear from Table 2, the drug entrapment efficiency of Mol-Ns formulations ranged from 71.45 ±1.69 to 95.63 ±1.50 %. The data confirms that, the effect of changing SAA type (X_1) &/or SAA: CH ratio (X_2) have significant effect on the EE % (Y_1) of the

produced Mol-Ns ($p<0.05$). When compared to Sp40, Sp60 exhibits the highest entrapment efficiency. Long-chain SAA cause significant entrapment, hence this could be related to the chemical structure of the surfactant. Furthermore, the alkyl chain length impacts the HLB value, which in turn decisively impacts the drug entrapment ability [24]. When niosomes made by Sp60 (HLB 4.7) and Sp40 (HLB 6.7) are concerned, the higher the drug entrapment efficiency and stability, the lower the HLB of the surfactant [25]. The results support the theory that a greater surfactant transition temperature (T_C) is associated with a higher EE%. This is consistent with the observation that Sp60, having a larger T_C than Sp40, allows for better drug entrapment. While drug leakage from niosomes may be prevented by maintaining ideal cholesterol to nonionic surfactant ratio of 1:1, which would result in enhanced EE%. [24]. Conversely, when the CH concentration was increased above what was necessary, there was a significant decrease in drug entrapment ($p > 0.05$). Where it might be due to either of the two reasons; hydrophobic medicine may have been trapped inside bilayers during vesicle formation at first, as permeability reduced and interlayer stability and hydrophobicity increased as the CH% increased. Overly high CH percentages provide a contradictory feature since they could compete with the drug for interlayer packing space [26, 27].

Table 2: 2^2 factorial design of Mol-Ns

Formulations	*Factors*		*Responses*		
	X_1: SAA type	*X_2: SAA: CH ratio*	*EE %(Y_1)*	*VS (n.m) (Y_2)*	*ZP (mV) (Y_3)*
Mol-N1	Sp60	1:1	95.36 ±1.5	92.215±6.0	-29.67±0.22
Mol-N2	Sp40		74.98 ±1.28	98.962±3.18	-21.25±0.82
Mol-N3	Sp60	1:2	82.14 ±0.82	101.672±5.64	-26.67±0.69
Mol-N4	Sp40		71.45 ±1.69	106.457±9.20	-19.68±0.73

Table 3: The dependent responses' ANOVA analysis

Responses	*S.S*	*df*	*MS*	*F-value*	*P-value*	*R^2*	*Adj. R^2*	*Pred. R^2*
EE %	646.90	3	215.63	237.15	< 0.0001	0.994	0.990	0.977
VS	352.53	3	111.71	26.04	0.0044	0.951	0.914	0.885
ZP	111.08	3	111.69	37.23	0.0007	0.981	0.967	0.924

SS: sum of square, df: Degree of freedom, MS: mean sum of square, R^2: determination coefficient, Adj. R^2: adjusted determination coefficient, Pred. R^2: predicted determination coefficient.

Statistical analysis of the independent parameters' effects on EE % studied by the experimental design ended up with the final equation:

EE% (Y_1) = +80.87 -7.31*A- 4.67 *B + 2.39 *A*B (2)

In line with the data shown in Table 3 and design data analysis, the model equation's coefficients indicated that altering the SAA type (X_1) had a greater impact on the EE% than altering the SAA:CH ratio (X_2). The model's significance is indicated by its F-value of 237.15, and its correlation coefficient (R^2) of 0.994 indicates that it is a well-fitting model. The factors interaction ($X_1.X_2$) had a substantial positive impact on Y_1, with a determined P-value of less than 0.0001.

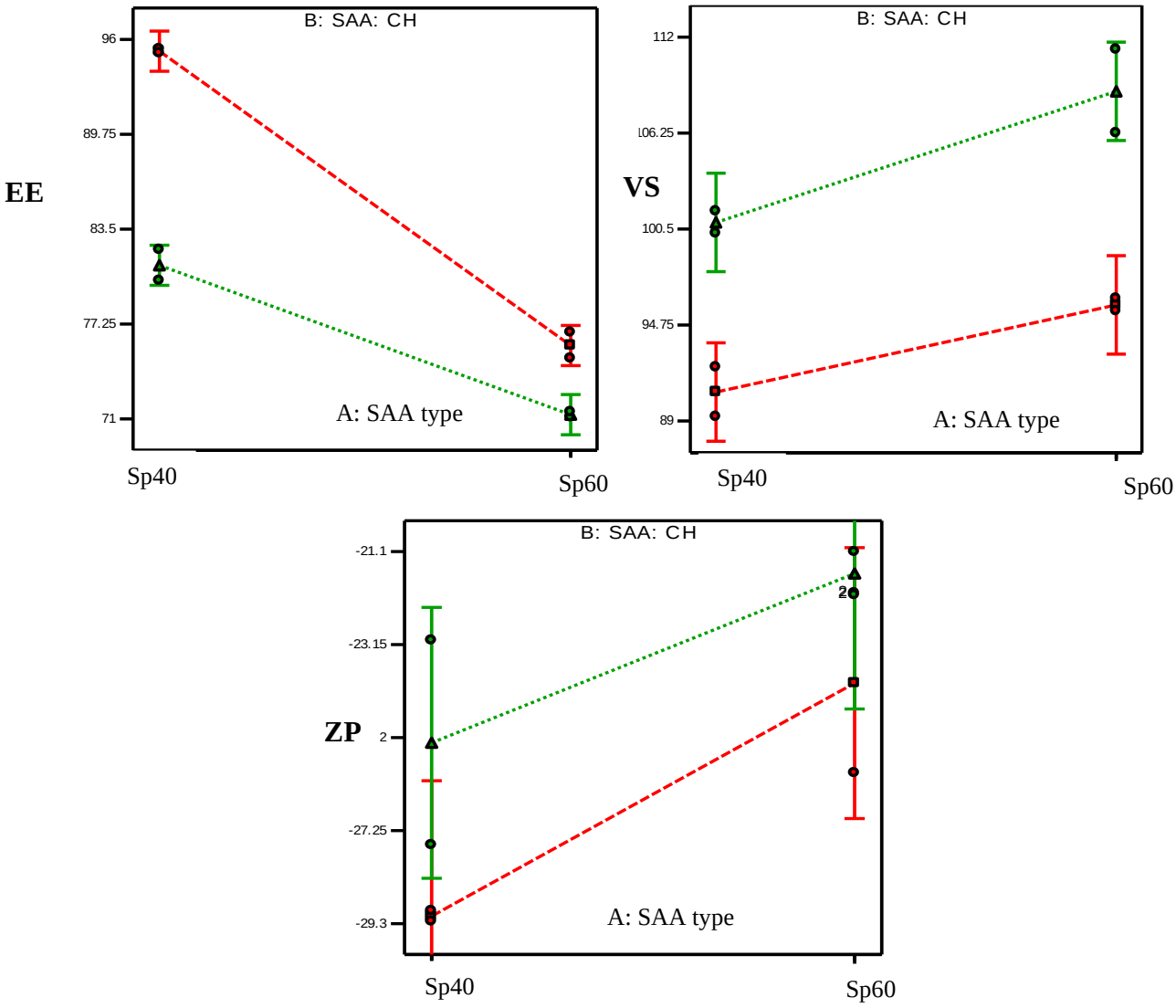

Figure 1: Design expert images showing factors effect and interactions on responses (a): on EE %, (b): VS, (c): ZP & (d): optimization desirability

3.2.2. Composition Variables' Impact on VS of Mol-Ns

In this study, all formulations exhibited sizes within the nanoscale range, measuring from 92.215±6.0 nm (Mol-N1) to 106.457±9.20 nm (Mol-N2) (Table 1). The findings confirmed a homogeneous and narrow distribution of vesicle sizes with favorable minimal polydispersity index values ranging from 0.37±0.16 to 0.57± 0.21. The findings indicate that niosomes made of surfactants with a lower HLB value should have smaller particle sizes than those made of surfactants with a higher HLB value, irrespective of cholesterol level [28, 29]. Likewise, regardless of the kind of surfactant employed, the size of the niosomes increased as the amount of CH incorporated into the formulation rose in terms of the SAA:CH ratio. These results corroborate the observations of *Khalil.,et al;* [26].

The statistical impact of independent factors on the VS:

VS (Y_2) = +99.08 + 3.7 * A+ 5.47 * B + 0.66 * A*B (3)

The influence of X_2 on the VS was higher than that of X_1, with a maximal coefficient estimate of 5.47. With an F-value of 26.04 and a correlation coefficient (R^2) = 0.951, the ANOVA analysis shown in Table 3 demonstrated a well-fitting model with a significant p-value of 0.0044.

3.2.3. Composition Variables' Impact on ZP of Mol-Ns

All niosomal vesicles' surface charges showed negative values, as indicated by Table 2. These values varied from -29.67±0.22 to -19.68±0.73 mv, signifying stable systems [25]. The outcomes were consistent with previous findings, which found that steady dispersion requires negative zeta potential levels greater than ±30 mV [20, 30]. The electric repulsion between the vesicles prevents the aggregation of the vesicles because of adequate charges.

The effect of independent factors on the ZP statistically:

ZP (Y_3) = -24.21 + 3.64 * A+ 0.87 * B + 0.020 * A*B (4)

Table 3's data demonstrated that the model with a correlation coefficient (R^2) = 0.981 and an F-value of 37.23 indicates significance and is an optimal match with a significant P-value < 0.0007.

3.3. Factorial design optimization of the produced Mol-Ns

Full factor design numerical optimization was used to optimize the formulations for the type of SAA (X_1) and SAA:CH ratio (X_2) that will minimize particle size and zeta potential while promoting EE% for essential efficiency. This was carried out in compliance with the data analysis provided for the factorial design. Desirability has a value between 0 and 1. The best formula is selected whenever the desirability value approaches 1. Mol-N1, which is made up of Sp60 in a 1:1 SAA:CH ratio, was discovered to be the best of the prepared niosomes, with a desirability value of 0.971. The most advantageous ZP (-29.67 mV), EE% (95.36 %), and particle size (92.25 nm) were displayed by Mol-N1.

3.4. Preparation of the Molnupiravir niosomal gel (Mol-NG1)

There were no impurities or suspended particles in any of the produced Molnupiravir gel, which was transparent and clear. An in situ gel formulation's viscosity should be adjusted to facilitate simple liquid dropping into the nasal cavity, which should be followed by an instantaneous gel phase. Hydroxyethyl cellulose (HEC) is one of the primary industrial cellulose derivatives with the potential to be used as a thickening agent. This kind of hydrogel can quickly transition between a liquid state at 25 °C to a hydrogel state at 37 °C, the body temperature [31].

3.5. Characterization of the optimized Mol-NG1

3.5.1. In vitro release study

The release characteristics of Molnupiravir from the medication solution, Mol-N1, and Mol-NG1 gel during a 12-hour investigation are shown in Figure 2.

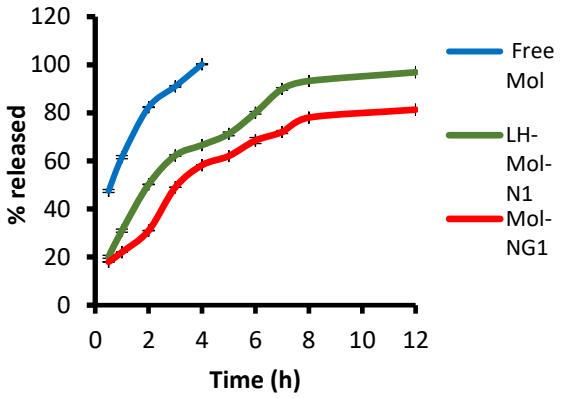

Figure 2: In vitro release profile In vitro drug release of Mol from free Mol, Mol-N1, and Mol-NG1

As found, the release profile showed that after three hours, free Mol had reached over 90%, as opposed to 60% and 40% with Mol-N1 and Mol-NG1, respectively. The observed outcome may be caused by Mol being incorporated into the formed niosomal vesicles' aqueous core, which prevents the medication from being released. Mol-NG1, the optimized formula, exhibited increased viscosity due to the hydrogel structure of HEC, which is noteworthy and believed to act as a barrier to slow down drug release [32]. This allowed for slower release compared to Mol-N1 and free drug solution, whereas the therapy must disperse via the gel structure before arriving the receptor media [32]. The desired mucoadhesive feature of HEC, the gelling agent derived from cellulose, allows the medications to remain in the nasal cavity for a significantly longer period of time [18]. Additionally, sustained release of the drug can be maintained due to the high viscosity of the cellulose following hydration in the nasal cavity [33].

3.5.2. Rheological study of Mol-NG1

In the preliminary stages of pharmaceutical research and development, rheology, the study of flow characteristics of semisolid formulations, aids in predicting spreadability of drug delivery systems [34]. For efficient and targeted medication administration, the viscosity of gel compositions must be acceptable. Figure 3(a&b) shows the correlation between the shear rate &shear stress of the Mol-NG1 gel formulation, which uses HEC as the gel excipient. As the shear rate grew, the gel's consistency progressively decreased, leading to an internal structure that became chaotic as the areas in contact broke, the particulates aligned, and the gel

started to flow. The internal structure of the system started to rebuild after the imposed stress was decreased, even though it took some time for the particles to interact and form the gel network. Formulas showed shear-thinning behavior, as indicated by the rheogram. This is advantageous for local drug delivery systems since the formulation flows readily at high shear rates upon gel application [35]. Furthermore, the downward slope of the rheogram showed that the gel's viscosity decreased with increasing shear rate, resulting in a prolonged drug residence time at the application site [32]. The visual appearance of the prepared selected Mol-NG1 is demonstrated in figure 3(c).

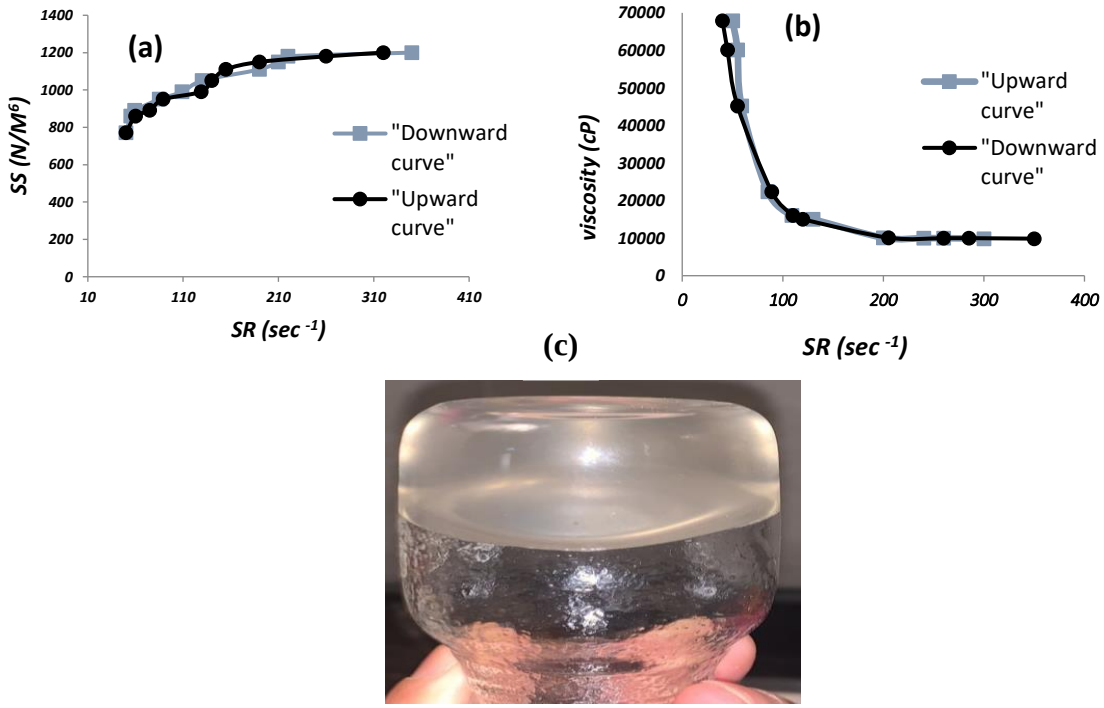

Figure 3: Shear stress (a) and viscosity (b) versus shear rate (sec $^{-1}$) of Mol-NG1, visual appearance of selected Mol-NG1

3.5.3. **pH Examination**

With a virtually neutral pH of 6.6, the optimized Mol-NG 1 looked uniform and smooth. This indicated that there wouldn't be any mucosal irritation because the pH was within an acceptable range [18].

3.5.4. **TEM Examination**

The development of Molnupiravir niosomal gels (Mol-NG1) is confirmed by TEM images displayed in Figure 4. The optimized Mol-NG1 was spherical and ranged in size from 100 nm to 200 nm on average, putting them in line with the DLS outcomes.

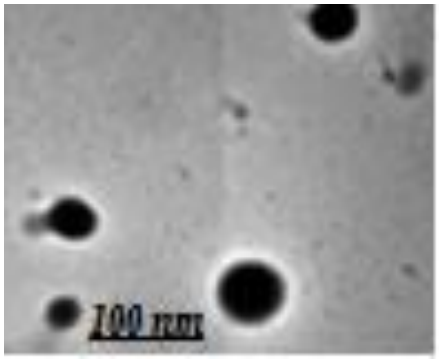

Figure 4: TEM image of Mol-NG1

3.6. In vivo study

3.6.1. **Mol-NG1's Impact on PI3K, AKT, TGF-β, and TNF-α**

$K_2Cr_2O_7$ activates multiple pathways, not only enhances lipoperoxidation and decreases antioxidant status, but also triggers TNF-α and IL-6 production that involved in cell proliferation and inflammatory response [36]. Furthermore, transformed growth factor β1 (TGF-β1), another profibrogenic cytokine generated by Parkinson's disease stimulates ALI and inflammation by inducing fibroblast proliferation and differentiation [37]. TGF-β inhibits the antioxidants catalase and superoxide dismutase, hence releasing ROS extents. Previous study reported TGF-β1 vital role in the pathophysiology of Parkinson's diseases induced lung damage [38]. Our results revealed that,

$K_2Cr_2O_7$ injection significantly elevated the lung content of TNF-α and TGF-β by 96% and 91% respectively compared to normal. Meanwhile, in free drug and Mol-NG1 groups, TNF-α level was significantly reduced by 37% and 46% and TGF-β levels was significantly decreased by 34% and 45% respectively, as compared to the $K_2Cr_2O_7$ group (P value < 0.05). In addition, Mol-NG1 administration reduced lung content of TNF-α and TGF-β by 15% and 17% respectively compared to the free drug group and returned TNF-α and TGF-β levels to their normal values as compared to the normal control group, as shown in figure 5 [39].

Intracellular phosphatidylinositol kinase (PI3K) phosphorylates protein kinase B and is linked with oxidative damage and apoptosis [40] PI3K provokes antioxidant genes expression [41]. PI3K/AKT promotes cellular growth, longevity and proliferation. Recently, its modulation is considered as an effective treatment for various diseases [42]. the current study showed a significant reduction in PI3K and AKT lung contents by 45% and 43% in the $K_2Cr_2O_7$ group as compared with the normal. Free drug and Mol-NG1 produced an elevation of the lung content of PI3K by 32% and 52% and AKT by 19% and 63%, respectively, compared to the $K_2Cr_2O_7$ group. Moreover, Mol-NG1 administration reduced lung content of PI3K and AKT by 15% and 38% respectively compared to the free drug group [43].

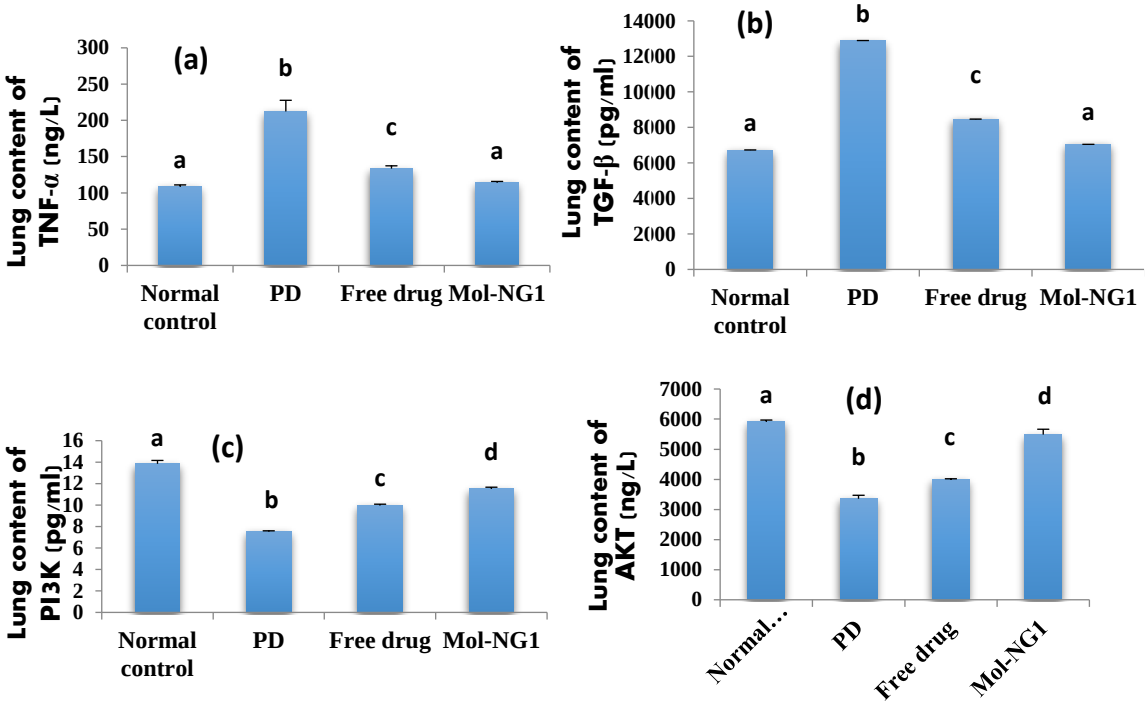

Figure 5: Effect of formula on (a): TNF-α, (b): TGF-β, (c): IP3K and (d): AKT.
For each parameter, same letter means non-significant difference, while different letter means significant difference at $p < 0.05$.

3.6.2. **Histopathological findings**

Rats in the normal control group displayed no histopathological changes and normal bronchiole with adjacent alveoli, while the rats in the positive group had severe blood vessel dilatation and congestion along with focal leucocyte aggregation and inflammatory cells observed in the parenchyma. In addition, there is proliferated focal peribronchiolar lymphoid cells aggregation associated with diffuse hemorrhage in most of the parenchyma,
air alveoli collapse and emphysema. The free drug group exhibited congestion which was observed in the peribronchiolar blood vessels; however Mol-NG1 group showed histopathological alteration as shown in figure 6.

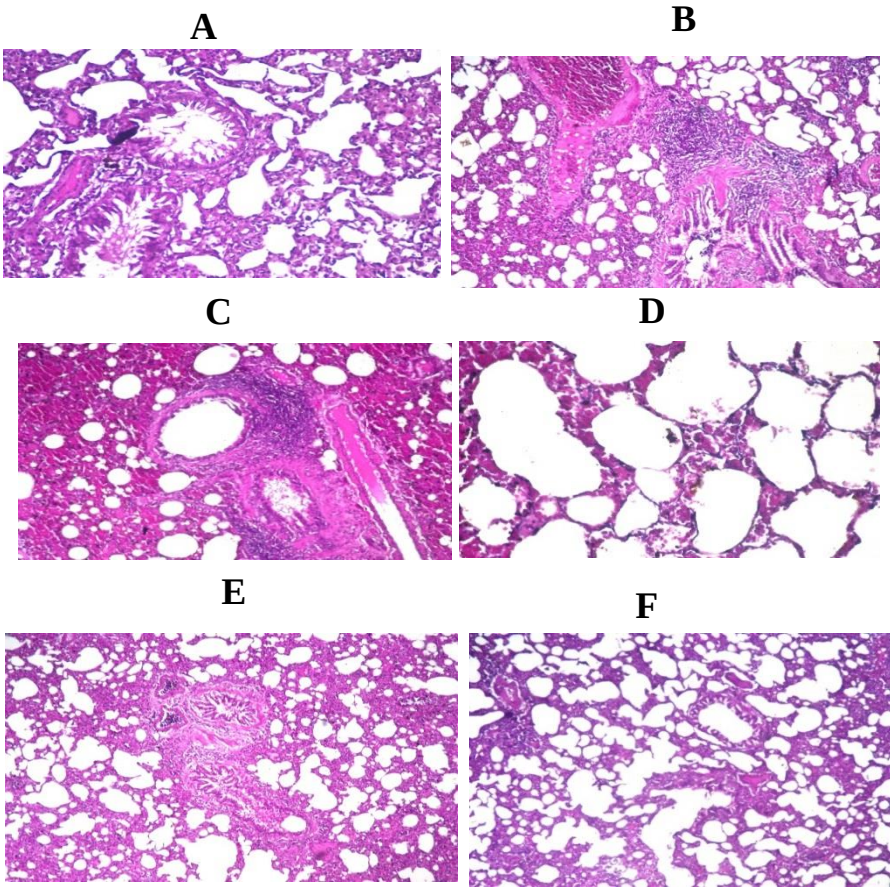

Figure 6: Histopathology of lung tissue A: Normal control, B, C, D: Positive control ($K_2Cr_2O_7$), E: Free drug, F: Mol-NG1

4. Conclusion

Molnupiravir's novel in situ niosomal nasal gels were manufactured by optimizing the SAA:CH ratio and the type of SAA employed. The tailored Mol-NG1 (Sp60, 1:1 ratio SAA: CH) was blended into HEC gels that had appropriate mechanical and rheological characteristics for nasal drug delivery. This helped to overcome the drug's low bioavailability. Given the in vivo outcomes, this composited hydrogel may greatly enhance Molnupiravir's therapeutic value. Mol-NG1 demonstrated superior healing results compared to normal control, positive control ($K_2Cr_2O_7$), and free radicals in an in vivo study that examined its effects on TNF-α, TGF-β, PI3K, and AKT in addition to histological analysis of rat lung tissue suffered an acute lung injury.

5. Conflict of interest

"There are no conflicts to declare".

6. Funding

"The authors declare that no funds, grants, or other support were received during the preparation of this manuscript."

7. Author Contributions

"All authors contributed to the study conception and design. Material preparation, data collection and analysis were performed by hadeer el hashemy, abeer salama and Amira rashad.

8. Acknowledgment

Authors acknowledge the support of national research Centre laboratories that has helped us executing the experimental studies.

9. References

1. Yang, J., et al., *Ginsenoside Rg3 Attenuates Lipopolysaccharide-Induced Acute Lung Injury via MerTK-Dependent Activation of the PI3K/AKT/mTOR Pathway.* Front Pharmacol, 2018. **9**(1): p. 1-13.
2. Torre, V.D., et al., *Acute respiratory distress syndrome in traumatic brain injury: how do we manage it?* J Thorac Dis, 2017. **9**(12): p. 5368-5381.
3. Sweeney, R.M. and D.F. McAuley, *Acute respiratory distress syndrome.* Lancet, 2016. **388**(1): p. 2416–2430.

4. Lu, Y., et al., *Potential "Therapeutic" Effects of Tocotrienol-Rich Fraction (TRF) and Carotene "Against" Bleomycin-Induced Pulmonary Fibrosis in Rats via TGF-ß/Smad, PI3K/Akt/mTOR and NF-κB Signaling Pathways.* Nutrients 2022, 14, 1094, 2022. **14**(1): p. 1094-1111.
5. Painter, W.P., et al., *Human Safety, Tolerability, and Pharmacokinetics of Molnupiravir, a Novel Broad-Spectrum Oral Antiviral Agent with Activity Against SARS-CoV-2.* Antimicrob Agents Chemother, 2021. **65**(5).
6. Imran, M., et al., *Discovery, Development, and Patent Trends on Molnupiravir: A Prospective Oral Treatment for COVID-19.* Molecules 2021. **26**(19): p. 1-18.
7. Kabinger, F., et al., *Mechanism of Molnupiravir-Induced SARS-CoV-2 Mutagenesis.* Nat Struct Mol Biol, 2021. **28**(9): p. 740-746.
8. Singh, A.K., et al., *Molnupiravir in COVID-19: A systematic review of literature.* Diabetes Metab Syndr, 2021. **15**(6): p. 1-12.
9. Cox, R.M., J.D. Wolf, and R.K. Plemper, *Therapeutically administered ribonucleoside analogue MK-4482/EIDD-2801 blocks SARS-CoV-2 transmission in ferrets.* Nat Microbiol 2021. **6**(1): p. 11-18.
10. Sheahan, T.P., et al., *An orally bioavailable broad-spectrum antiviral inhibits SARS-CoV-2 in human airway epithelial cell cultures and multiple coronaviruses in mice.* Sci Transl Med, 2020. **12**(541): p. 1-20.
11. Abou-Taleb, H.A., R.A. Khallaf, and J.A. Abdel-Aleem, *Intranasal niosomes of nefopam with improved bioavailability: Preparation, optimization, and in-vivo evaluation.* Drug Des Devel Ther, 2018. **12**(1): p. 3501–3516.
12. Fahmy , U.A., et al., *Intranasal Niosomal In Situ Gel as a Promising Approach for Enhancing Flibanserin Bioavailability and Brain Delivery: In Vitro Optimization and Ex Vivo/In Vivo Evaluation.* Pharmaceutics, 2020. **12**(6): p. 1-23.
13. Ge, X., et al., *Advances of Non-Ionic Surfactant Vesicles (Niosomes) and Their Application in Drug Delivery.* Pharmaceutics, 2019. **12**(1): p. 485-508.
14. FitzGerald, R., et al., *Pharmacokinetics of ß-d-N4-Hydroxycytidine, the Parent Nucleoside of Prodrug Molnupiravir, in Nonplasma Compartments of Patients With Severe Acute Respiratory Syndrome Coronavirus 2 Infection.* Clin Infect Dis, 2022. **75**(1): p. 525-528.
15. Laurini, G.S., N. Montanaro, and D. Motola, *Safety Profile of Molnupiravir in the Treatment of COVID-19: A Descriptive Study Based on FAERS Data.* J Clin Med, 2022. **12**(1): p. 34-42.
16. Kim, D., Y.H. Kim, and S. Kwon, *Enhanced Nasal Drug Delivery Efficiency by Increasing Mechanical Loading Using Hypergravity.* Sci Rep, 2018. **8**(1): p. 168-176.
17. Marzouk, M.A., et al., *Pharmacokinetic Study of Mucoadhesive Itopride Hydrochloride In Situ Nasal Gel Formulations in a Comparative In Vivo Study and Histopathological Safety Evaluation.* Sci Pharm, 2022. **90**(1): p. 8-18.
18. Sherafudeen, S.P. and P.V. Vasantha, *Development and evaluation of in situ nasal gel formulations of loratadine.* Res Pharm Sci, 2015. **10**(6): p. 466-76.
19. Chettupalli, A.K., et al., *Design, Formulation, In-Vitro and Ex-Vivo Evaluation of Atazanavir Loaded Cubosomal Gel.* Biointerface Res Appl Chem, 2021. **11**(4): p. 12037 - 12054.
20. El-Hashemy, H.A., *Design, formulation and optimization of topical ethosomes using full factorial design: in-vitro and ex-vivo characterization.* J Liposome Res, 2022. **32**(1): p. 74-82.
21. Tanbek K and S. S., *Dose-dependent Oxidative Damage of Molnupiravir (Antiviral Drug for Treatment of COVID-19) in Lung, Liver, Heart, and Kidney Tissues in Rats.* Arch Pharmacol Ther., 2023. **5**(1): p. 44-52.
22. Salama, A., et al., *Impact of protocatechuic acid on alleviation of pulmonary damage induced by cyclophosphamide targeting peroxisome proliferator activator receptor, silent information regulator type ⁻1, and fork head box protein in rats.* Inflammopharmacology, 2023. **31**(1): p. 1361–1372.
23. Banchroft , J.D., C. Layton, and S.K. Suvarna *Bancrofts theory and practice of histological techniques*. Seven th ed. 2013, New York: Elisevser.
24. Abdelbary, G. and N. El-Gendy, *Niosome-encapsulated gentamicin for ophthalmic controlled delivery.* AAPS PharmSciTech, 2008. **9**(3): p. 740-747.
25. Teaima, M.H., et al., *Formulation and evaluation of niosomal vesicles containing ondansetron HCL for trans-mucosal nasal drug delivery.* Drug Dev Ind Pharm, 2020. **46**(5): p. 751-761.

26. Khalil, R.M., et al., *Evaluation of bilosomes as nanocarriers for transdermal delivery of tizanidine hydrochloride: in vitro and ex vivo optimization.* J Liposome Res, 2019. **29**(2): p. 171-182.
27. El-Menshawe, S.F. and A.K. Hussein, *Formulation and evaluation of meloxicam niosomes as vesicular carriers for enhanced skin delivery.* Pharm Dev Technol, 2011. **18**(4): p. 779-786.
28. El-Hashemy, H.A., A. Salama, and A. Rashad, *Experimental design, formulation, and in-vivo evaluation of novel anticoagulant Rivaroxaban loaded cubosomes in rats model.* J Liposome Res, 2023. **33**(2): p. 189-196.
29. Mohsen, A.M., et al., *Formulation of tizanidine hydrochloride-loaded provesicular system for improved oral delivery and therapeutic activity employing a 2(3) full factorial design.* Drug Deliv Transl Res, 2023. **13**(2): p. 580-592.
30. Khalil, R.M., et al., *Development of tizanidine loaded aspasomes as transdermal delivery system: ex-vivo and in-vivo evaluation.* J Liposome Res, 2021. **31**(1): p. 19-29.
31. Yao, M., et al., *Chitosan-based thermosensitive composite hydrogel enhances the therapeutic efficacy of human umbilical cord MSC in TBI rat model.* Materials Today Chemistry, 2019. **14**: p. 100192.
32. Ho, H.N., et al., *Formulation and characterization of hydroxyethyl cellulose-based gel containing metronidazole-loaded solid lipid nanoparticles for buccal mucosal drug delivery.* Int J Biol Macromol, 2022. **194**: p. 1010-1018.
33. Chaturvedi, M., M. Kumar, and K. Pathak, *A review on mucoadhesive polymer used in nasal drug delivery system.* J Adv Pharm Technol Res, 2011. **2**(4): p. 215-22.
34. Marques, A.C., et al., *Development and characterization of mucoadhesive buccal gels containing lipid nanoparticles of ibuprofen.* International Journal of Pharmaceutics, 2017. **533**(2): p. 455-462.
35. El-Hashemy, H.A., *Design, formulation and optimization of topical ethosomes using full factorial design: in-vitro and ex-vivo characterization.* J Liposome Res, 2022. **32**(1): p. 74-82.
36. Salama, A. and R. Elgohary, *L-carnitine and Co Q10 ameliorate potassium dichromate - induced acute brain injury in rats targeting AMPK/AKT/NF-κβ.* Int Immunopharmacol, 2021. **101**(B): p. 1-15.
37. Fahy, R.J., et al., *The acute respiratory distress syndrome: a role for transforming growth factor-beta 1.* Am J Respir Cell Mol Biol, 2003. **28**(4): p. 499–503.
38. Salama, A., H.M. Fayed, and R. Elgohary, *L-carnitine alleviated acute lung injuries induced by potassium dichromate in rats: involvement of Nrf2/HO-1 signaling pathway.* Heliyon, 2021. **7**(6): p. 1-9.
39. Jiang, Y., et al., *Inflammatory pathways in COVID-19: Mechanism and therapeutic interventions.* MedComm (2020), 2022. **3**(3): p. e154.
40. Rushmi, Z.T., et al., *The impact of formulation attributes and process parameters on black seed oil loaded liposomes and their performance in animal models of analgesia.* Saudi Pharm J, 2017. **25**(3): p. 404-412.
41. Zhang, X.L., et al., *DJ-1 regulating PI3K-Nrf2 signaling plays a significant role in bibenzyl compound 20C-mediated neuroprotection against rotenone-induced oxidative insult.* Toxicol Lett, 2017. **271**(1): p. 74–83.
42. Salama, A., R. Mostafa, and R. Elgohary, *Effect of L-carnitine on potassium dichromate-induced nephrotoxicity in rats: modulation of PI3K/AKT signaling pathway.* Res Pharm Sci, 2022. **17**(2): p. 153-163.
43. Martínez, A., *Electron Donor-Acceptor Capacity of Selected Pharmaceuticals against COVID-19.* Antioxidants (Basel), 2021. **10**(6).